

Split-gate quantum point contacts with tunable channel length

M. J. Iqbal,^{1,a)} J. P. de Jong,¹ D. Reuter,² A. D. Wieck,² and C. H. van der Wal¹

¹Zernike Institute for Advanced Materials, Nijenborgh 4, University of Groningen, NL-9747AG Groningen, The Netherlands

²Angewandte Festkörperphysik, Ruhr-Universität Bochum, D-44780 Bochum, Germany

(Received 4 July 2012; accepted 17 December 2012; published online 10 January 2013)

We report on developing split-gate quantum point contacts (QPCs) that have a tunable length for the transport channel. The QPCs were realized in a GaAs/AlGaAs heterostructure with a two-dimensional electron gas (2DEG) below its surface. The conventional design uses 2 gate fingers on the wafer surface which deplete the 2DEG underneath when a negative gate voltage is applied, and this allows for tuning the width of the QPC channel. Our design has 6 gate fingers and this provides additional control over the form of the electrostatic potential that defines the channel. Our study is based on electrostatic simulations and experiments and the results show that we developed QPCs where the effective channel length can be tuned from about 200 nm to 600 nm. Length-tunable QPCs are important for studies of electron many-body effects because these phenomena show a nanoscale dependence on the dimensions of the QPC channel. © 2013 American Institute of Physics. [<http://dx.doi.org/10.1063/1.4774281>]

I. INTRODUCTION

A quantum point contact (QPC) is the simplest mesoscopic device that directly shows quantum mechanical properties. It is a short ballistic transport channel between two electron reservoirs, which shows quantized conductance as a function of the width of the channel.^{1,2} A widely applied approach for implementing QPCs is using a split-gate structure on the surface of a heterostructure with a two-dimensional electron gas (2DEG) at about 100 nm beneath its surface. The conventional design of such a split-gate QPC has two metallic gate fingers (Fig. 1(a)). Operating this device with a negative gate voltage V_g results in the formation of a barrier with a small tunable opening between two 2DEG reservoirs, because the 2DEG below the gate fingers gets depleted over a range that depends on V_g . For electrons in the 2DEG, this appears as an electrostatic potential U that is a large barrier with a small opening in the form of a saddle-point potential (Fig. 3). The saddle-point potential gives transverse confinement in the channel that is roughly parabolic, which results for this transverse direction in a discrete set of electronic energy levels. For electron transport along the channel, this gives a discrete set of subbands with one-dimensional character. Quantized conductance appears because each subband contributes $G_0 = 2e^2/h$ to the channel's conductance,^{1,2} where e is the electron charge and h is Planck's constant.

We present here the design and experimental characterization of QPCs which offer additional control over the shape of the saddle-point potential. We focused on developing devices for which the effective length of the saddle-point potential (along the transport direction) can be tuned *in situ*. The additional control is implemented with a symmetric split-gate design based on 6 gate fingers (Fig. 1(b)). Such devices will be denoted as QPC_{6F} and conventional devices

with 2 gate fingers (Fig. 1(a)) as QPC_{2F}. These QPC_{6F} are operated with the gate voltage on the outer fingers (V_{g2}) less negative than the gate voltage on the central fingers (V_{g1}) to avoid quantum dot formation. Sweeping V_{g1} from more to less negative values opens the QPC_{6F}. By co-sweeping V_{g2} at fixed ratio V_{g2}/V_{g1} it behaves as a QPC with a certain length for the saddle-point potential, and this length can be chosen by setting V_{g2}/V_{g1} : It is shortest for $V_{g2}/V_{g1} \approx 0$ and longest for $V_{g2}/V_{g1} \lesssim 1$. For our design, the effective length could be tuned from about 200 nm to 600 nm.

The motivation for developing these length-tunable QPCs comes from studies of electron many-body effects in QPCs. A well-known manifestation of these many-body effects is the so-called 0.7 anomaly,³ which is an additional shoulder at $0.7G_0$ in quantized conductance traces. These many-body effects are, despite many experimental and theoretical studies since 1996,⁴ not yet fully understood. Recent theoretical work⁵ suggested that many-body effects cause the formation of one or more self-consistent localized states in the QPC channel, and that these effects result in the 0.7 anomaly and the other signatures of many-body physics. This theoretical work predicted a clear dependence on the length of the QPC channel, and testing this directly requires experiments where this length is varied.

The work by Koop *et al.*⁶ already explored the relation between the device geometry and parameters that describe the many-body effects in a large set of QPC_{2F} devices. This work compared nominally identical devices, and devices for which the lithographic length L_{litho} (see Fig. 1(a)) and width of the channel in the split-gate structure were varied. These results were, however, not conclusive. The parameters that describe the many-body effects showed large, seemingly random variation, not correlated with the device geometry. At the same time, the devices showed (besides the 0.7 anomaly) clean quantized conductance traces, and the parameters that reflect the non-interacting electron physics did show the variation that one expects when changing the geometry (for

^{a)}e-mail: javaid2k@gmail.com.

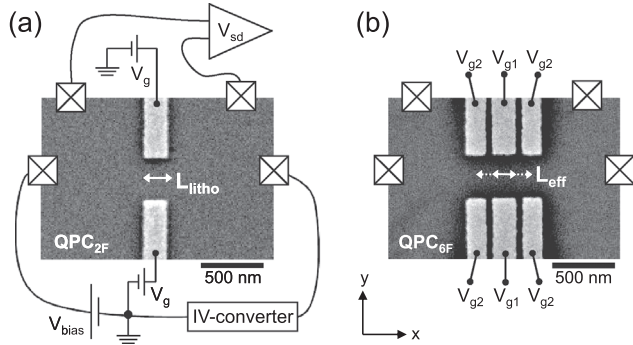


FIG. 1. (a) SEM image of a conventional split-gate quantum point contact (QPC). It has two gate fingers (QPC_{2F} device). The length of the QPC channel is fixed and can be parameterized by the lithographic length L_{litho} of the gate structure. The diagram also illustrates the measurement scheme. (b) SEM image of a length tunable QPC with 6 gate fingers (QPC_{6F} device). Here, the effective length L_{eff} of the QPC can be tuned by changing the ratio of the gate voltages on the central gates (V_{g1}) and side gates (V_{g2}).

example, the channel pinch-off gate voltage V_{po} and subband spacing $\hbar\omega_{12}$). This confirms that these QPCs had saddle-point potentials that were smooth enough for showing quantized conductance, while it also shows that the many-body effects are very sensitive to small static fluctuations on these saddle-point potentials or to nanoscale device-to-device variations in the dimensions of the potentials. This picture was confirmed by shifting the channel position inside a particular QPC_{2F} device. This can be implemented by operating a QPC_{2F} with a difference ΔV_g between the values of V_g on the two gate fingers in Fig. 1(a). Such a channel shift did not change the quantized conductance significantly but did cause strong variation in the signatures of many-body physics. Earlier work had established that such device-to-device fluctuations can be due to remote defects or impurities, a slight variation in electron density or due to the nanoscale variation in devices that is inherent to the nanofabrication process.^{6–8} Consequently, studying how the many-body effects depend on the length of the QPC channel requires QPCs for which the channel length can be tuned continuously *in situ*, and where this can be operated without a transverse displacement of the QPC channel in the semiconductor material. The work that we report here aimed at realizing such devices.

This article is organized as follows: Section II starts with a short overview of the options and the choices we made for realizing the QPC_{6F} devices. Next, in Sec. III, we present the results of electrostatic simulations. In Sec. IV, we describe the sample fabrication and measurement techniques. This is followed by comparing results from simulations and experiments for QPC_{6F} devices in Sec. V, and Sec. VI summarizes our conclusions.

II. DESIGN CONSIDERATIONS

We designed our QPC_{6F} devices with 6 rectangular gate fingers, in a symmetric layout with two sets of 3 parallel gate fingers (Figs. 1(b) and 2(a)). SEM inspection of fabricated devices yields that the central gate finger is 200 nm wide (as measured along the direction of channel length L_{eff}). The outer gate fingers are 160 nm wide, and the narrow gaps between gate fingers are 44 nm wide. This yields

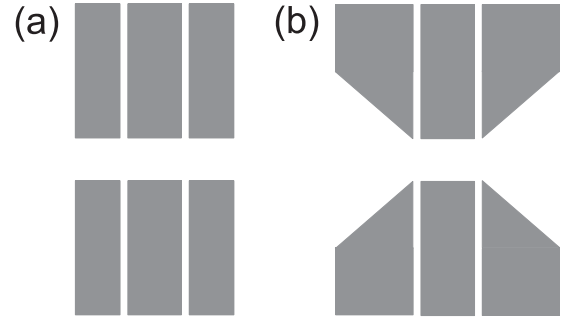


FIG. 2. (a) Design of the geometry of the 6 gate fingers for a QPC_{6F} device with 6 rectangular gate fingers. (b) Design of a QPC_{6F} device with the 4 outer gates in a shape that explicitly induces a funnel shape for the entry and exit of the QPC transport channel.

$(200 + 2 \cdot 160 + 2 \cdot 44) \text{ nm} = 608 \text{ nm}$ for the total distance between the outer sides of the 3 parallel gate fingers. The lithographic width of the QPC channel (distance between the two sets of 3 gate fingers) is 350 nm.

An example of alternative designs for the gate geometries that we considered is in Fig. 2(b). This design has a two-sided funnel shape for the channel and this could result in length-tunable QPC operation that better maintains a regular shape for the saddle-point potential. However, the electrostatic simulations in Sec. III show that the rectangular gate fingers as in Fig. 2(a) also give a length-tunable saddle-point potential that maintains a regular shape while tuning the length. This observation holds for a range of device dimensions similar to our design. For our particular design, the lithographic length and width (350 nm) of the channel are comparable, and the 2DEG is as far as 110 nm distance below the surface (and the part in the center of the channel that actually contains electrons is very narrow, about 20 nm). In this regime, the saddle-point potential is strongly rounded with respect to the lithographic shapes of the gates (see for example Figs. 3(c) and 3(d)). An important advantage of the rectangular design is that it provides two clear points for calibrating the effective channel length L_{eff} : Operating at $V_{g2}/V_{g1} = 0$ gives $L_{eff} = L_{litho}$ for the central gate finger alone (200 nm, see Fig. 1(b)), while operating at $V_{g2}/V_{g1} = 1$ gives L_{eff} equal to the lithographic distance between the outer sides of the 3 parallel gate fingers (608 nm).

A point of concern for this design that deserves attention is whether the narrow gaps between the 3 parallel gate fingers induce significant structure on the saddle-point potential. The electrostatic simulations show that this is not the case (see again the examples in Figs. 3(c) and 3(d)). The part of the channel that contains electrons is relatively far away from the gate electrodes, and the potential U at this location is strongly rounded. Notably, the full height of the potentials in Fig. 3 is about 1 eV, while the occupied subbands are at a height of only about 10 meV above the stationary point of the saddle-point potential (in the center of the channel). Such gaps between parallel gate electrodes can be much narrower when depositing a wider gate on top of the central gate, with an insulating layer between them. We chose against applying this idea since we also aimed to have devices with a very low level of noise and instabilities from charge fluctuations

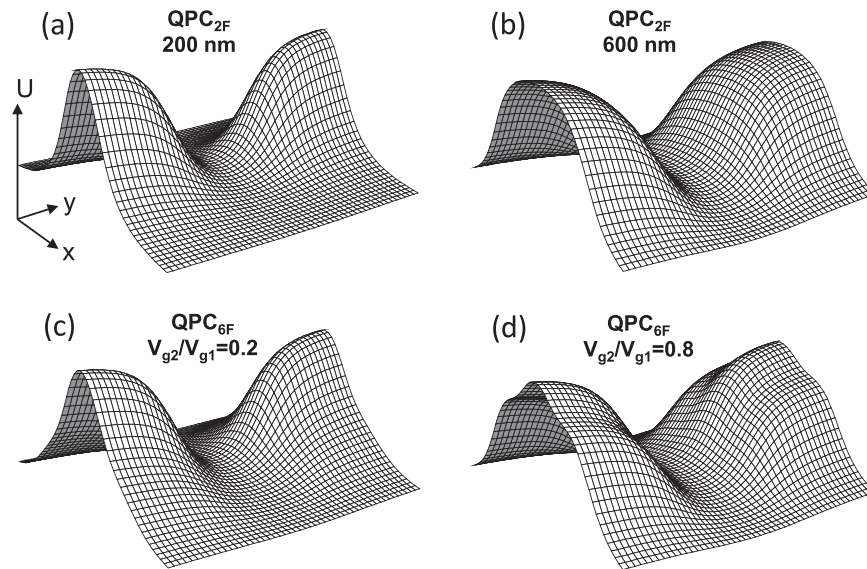


FIG. 3. (a) and (b) Saddle-point potentials that represent the electrostatic potential U felt by electrons in the 2DEG plane. The plots represent an area of $1000 \times 1000 \text{ nm}^2$, centered at the middle of a QPC channel with a length L_{litho} of 200 nm (a) and 600 nm (b) of a QPC_{2F} device with a lithographic channel width of 350 nm. It is calculated for the material parameters that are valid for the measured devices. See Fig. 1(b) for relating the x - and y -direction to the gate geometry. (c) and (d) Similar saddle-point potentials U calculated for QPC_{6F} devices (with material parameters and geometry as the measured devices). The effective channel length is shorter for the case that is calculated for $V_{g2}/V_{g1} = 0.2$ (c) than for the case $V_{g2}/V_{g1} = 0.8$ (d) (also note that QPC_{6F} results for $V_{g2}/V_{g1} = 0$ are the same as plot (a)). Panels (c) and (d) also show that the narrow gaps between 3 parallel gate fingers do not induce significant structure at low energies in the saddle-point passage (it only induces a weak fingerprint off to the side in the channel, at energies that are much higher than the occupied electron levels, see panel (d)).

at defect and impurity sites in the device materials. In this respect, we expect better behavior when all gate fingers are deposited in a single fabrication cycle, and when deposition of an insulating oxide or polymer layer can be omitted.

III. ELECTROSTATIC SIMULATIONS

This section presents results of electrostatic simulations of the saddle-point potentials that define the QPC channel. The focus is on the design with 6 rectangular gate fingers (Fig. 2(a)), with gate dimensions as mentioned in the beginning of Sec. II. The simulations are based on the modeling approach that was introduced by Davies *et al.*⁹

A. Davies' method for simulating 2DEG electrostatics

Davies *et al.*⁹ introduced a method for modeling the electrostatics of gated 2DEG. It calculates the electrostatic potential U for electrons in the 2DEG regions around the gates (the approach only applies to the situation where the 2DEG underneath the gates is depleted due to a negative voltage on gate electrodes). There are other models and approaches^{8,10–13} for calculating such potential landscapes, but these are all more complicated and computationally more demanding. The approach by Davies *et al.* is relatively simple. It does not account for electrostatic screening effects, and, notably, it does not account for the electron many-body interactions that were mentioned earlier. Still, it was shown that it is well suited for calculating a valid picture of a QPC saddle-point potential near the channel pinch-off situation.⁶

The negative voltage on a gate that is needed to exactly deplete 2DEG underneath a large gate is called the threshold voltage V_t , and it is to a good approximation given by

$$V_t = \frac{-en_{2D}d}{\epsilon_r\epsilon_0}. \quad (1)$$

Here n_{2D} is the electron density in the 2DEG (at zero gate voltage), d is the depth of the 2DEG, ϵ_r is the relative dielectric constant of the material below the gate, and ϵ_0 is the dielectric constant of vacuum (for details see Refs. 6 and 9). The value of V_t for a certain 2DEG material defines the value U_0 where the electrostatic potential U for electrons in the 2DEG becomes higher than the chemical potential of the 2DEG. In turn, this can be used to define in an arbitrary potential landscape U (for arbitrary gates shapes and for arbitrary gate voltages) the positions where $U = U_0$. That is, one can calculate the positions in a gated device structure where there is a boundary between depleted and non-depleted 2DEG and also calculate the electrostatic potential U around such points. When the center of the QPC has $U = U_0$, the channel is at pinch-off and no electrons can pass through the QPC. The gate voltage at which this happens is called the pinch-off voltage V_{po} . Notably, the calculated value of U at a certain position is simply the superposition of all the contributions to U from different gate electrodes, and it is linear in the gate voltage on each of these electrodes.⁹

Figure 3 presents examples of saddle-point potentials U that are calculated with Davies' method, both for QPC_{2F} and QPC_{6F} devices. The calculations are for material parameters and geometries of measured devices (as described in detail in Secs. IV and V). Figures 3(c) and 3(d) show that the length of the transport channel depends on the applied ratio V_{g2}/V_{g1} , and that the narrow gaps between 3 parallel electrodes in QPC_{6F} devices do not give significant structure on the saddle-point potential in the operation regime that we consider.

B. Definition and tuning of the effective length L_{eff}

The focus of this work is on realizing QPC channels with a tunable length. The channels are in fact saddle-point potentials (see Fig. 3), and it is for such a smooth shape not obvious on the value of the channel length. We therefore characterize this channel length with the parameter L_{eff} , which corresponds to the value of the lithographic length L_{litho} of a QPC_{2F} type device (with rectangular gate electrodes, see Fig. 1(a)) that gives effectively the same saddle-point potential.

We implemented this as follows. We calculated the saddle-point potential $U(x, y)$ for the pinch-off situation (see Figs. 1(b) and 3(a) for how the x - and y -directions are defined). The transverse confinement in the middle of the QPC (defined as $x=0, y=0$) is parabolic to a very good approximation. When moving out of the channel along the x -direction, the transverse confinement becomes weaker, but remains at first parabolic. Notably, the energy eigenstates for confinement in such a parabolic potential, described as

$$U(y) = \frac{1}{2} m^* \omega_0^2 y^2 \quad (2)$$

have a width that is (for all levels) proportional to $\omega_0^{-1/2}$. In this expression, m^* is the effective mass of the electron and ω_0 is the angular frequency of natural oscillations in this

potential. The parameter ω_0 defines here the steepness of $U(y)$, and we obtain $\omega_0(x)$ values from fitting Eq. (2) to potentials $U(x, y)$ obtained with Davies's method. We use this and investigate the width $\Delta y(x)$ in y -direction for the lowest energy eigenstate, at all positions x along the channel (see Fig. 4(a)). For parabolic confinement, this wavefunction in y -direction has a Gaussian shape and has a width

$$\Delta y(x) = \sqrt{\frac{h}{4\pi m^* \omega_0(x)}}. \quad (3)$$

With this approach, we analyzed that the distance from $x=0$ to the x -position x_α where the value $\Delta y(x)$ increased by a factor $\alpha \approx 1.1$ defines a suitable point for defining the value of L_{eff} . That is, we define

$$L_\alpha = 2x_\alpha \quad (4)$$

and find x_α by solving

$$\Delta y(x = x_\alpha) = \alpha \cdot \Delta y(x = 0) \quad (5)$$

for a certain α . Subsequently, L_{eff} is defined by using the suitable α value,

$$L_{eff} = L_\alpha \text{ for } \alpha = 1.1. \quad (6)$$

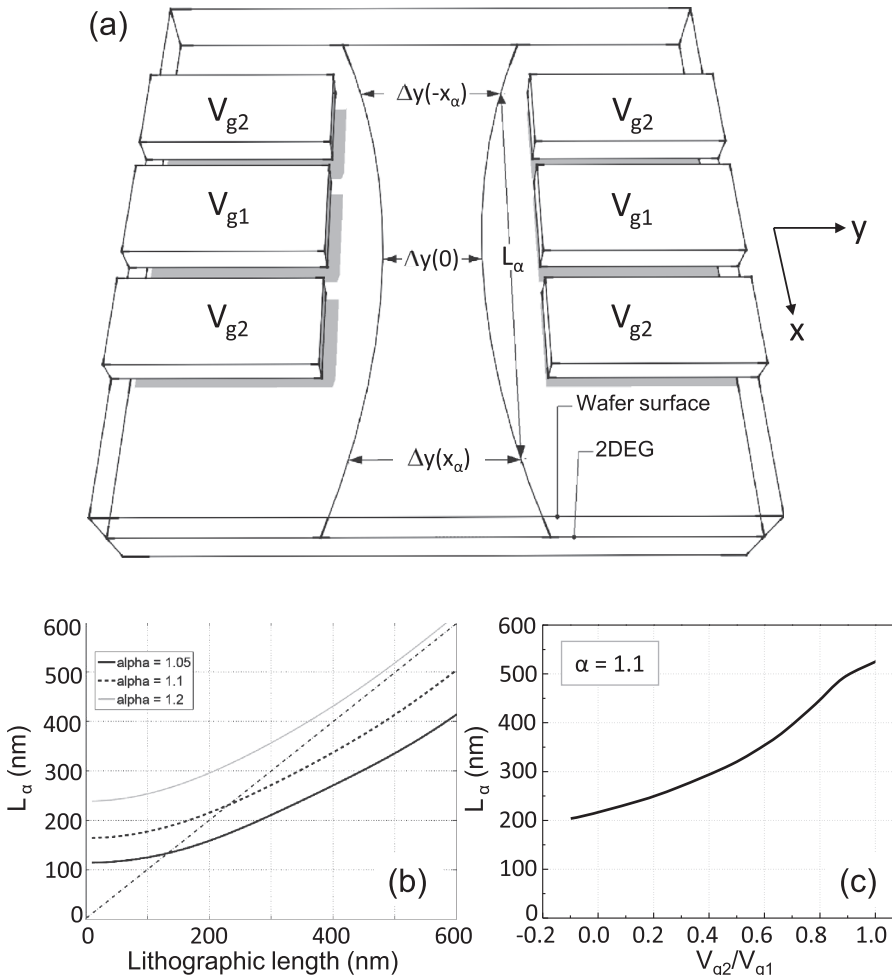


FIG. 4. (a) Schematic representation of a QPC_{6F} device, illustrating length variables: $\Delta y(x)$ is the width of the ground-state wavefunction at position x in the channel and L_α is twice the distance from the QPC center to the position x where $\Delta y(x)$ is a factor α wider. (b) The calculated length L_α for a range of values of the lithographic length of QPC_{2F} devices, for three values of α . (c) The calculated effective length L_α for $\alpha = 1.1$ for a QPC_{6F} device, as a function of the ratio V_{g2}/V_{g1} .

We came to this parameterization as follows. We used this *ansatz* first in simulations of QPC_{2F} devices. Here, we explored for different values of α the relation between L_{litho} and L_α . Results of this for $\alpha = 1.05, 1.1, \text{ and } 1.2$ are presented in Fig. 4(b). For the range of L_{litho} values that is of interest to our study (~ 100 nm to ~ 500 nm), we find the most reasonable overall agreement between the actual value for L_{litho} (input to the simulation) and the value L_α (derived from the simulation) for $\alpha = 1.1$. The agreement is not perfect, but we analyzed that the deviation is within an uncertainty that we need to assume because the exact shapes of saddle-point potentials in different device geometries do show some variation, and because of the limited validity of Davies' method. Nevertheless, it provides a reasonable recipe for assigning a value L_{eff} to any saddle-point potential, with at most 20% error.

Fig. 4(c) presents results of calculating $L_\alpha = L_{eff}$ for $\alpha = 1.1$ from simulations of a QPC_{6F} device, operated at different values for V_{g2}/V_{g1} . The results show a clear monotonic trend, with $L_{eff} = 210$ nm for $V_{g2}/V_{g1} = 0$ to $L_{eff} = 525$ nm for $V_{g2}/V_{g1} = 1$. This is for a QPC_{6F} device for which we expect $L_{eff} = 200$ nm for $V_{g2}/V_{g1} = 0$ and $L_{eff} = 608$ nm for $V_{g2}/V_{g1} = 1$ (see Sec. II). In Sec. V, we discuss how this latter point is used for applying a small correction to the simulated values for L_{eff} . These simulations show that the QPC_{6F} that we consider allows for tuning L_{eff} by about a factor 3.

It is worthwhile to note that our current design showed optimal behavior in the sense that it can tune L_{eff} from about 200 nm to 600 nm, while the dependence of L_{eff} on V_{g2}/V_{g1} is close to linear. We also simulated QPC_{6F} devices with wider gate electrodes for the outer gates and (as mentioned in Sec. II) devices with gate geometries as in Fig. 2(b). These devices showed a steeper slope for part of the relation between V_{g2}/V_{g1} and L_{eff} , which is not desirable.

IV. SAMPLE FABRICATION AND MEASUREMENT TECHNIQUES

We fabricated QPC devices with a GaAs/Al_{0.35}Ga_{0.65}As MBE-grown heterostructure, which has a 2DEG at 110 nm depth below its surface from modulation doping. The layer sequence and thickness of the materials from top to bottom (i.e., going into the material) starts with a 5 nm GaAs capping layer, then a 60 nm Al_{0.35}Ga_{0.65}As layer with Si doping at about $1 \times 10^{18} \text{ cm}^{-3}$, which is followed by an undoped spacer layer of 45 nm. The 2DEG is located in a heterojunction quantum well at the interface with the next layer, which is a 650 nm undoped GaAs layer. This heterostructure was grown on a commercial semi-insulating GaAs wafer, after first growing a sequence of 10 GaAs/AlAs layers for smoothing the surface and trapping impurities. The 2DEG had an electron density $n_{2D} = 1.6 \times 10^{15} \text{ m}^{-2}$ and a mobility $\mu = 118 \text{ m}^2 \text{ V}^{-1} \text{ s}^{-1}$. We fabricated both conventional QPC_{2F} devices and QPC_{6F} devices by standard electron-beam lithography and clean-room techniques. The gate fingers were deposited using 15 nm Au on top of a 5 nm Ti sticking layer. For measuring transport through the QPCs, we realized ohmic contacts to the 2DEG reservoirs by

annealing of a AuGe/Ni/Au stack that was deposited on the wafer surface.¹⁴ The geometries of the fabricated devices were already described in the beginning of Sec. II.

The measurements were performed in a He-bath cryostat and in a dilution refrigerator, thus getting access to effective electron temperatures from 80 mK to 4.2 K. We used standard lock-in techniques with an a.c. excitation voltage $V_{bias} = 10 \mu\text{V}$ RMS at 387 Hz. Fig. 1(a) shows the 4-probe voltage-biased measurement scheme, where both the current and the actual voltage drop V_{sd} across the QPC channel are measured such that any influence of series resistances could be removed unambiguously. The gate voltages are applied with respect to a single grounded point in the loop that carries the QPC current.

V. EXPERIMENTAL REALIZATION OF LENGTH-TUNABLE QPCs

This section presents an experimental characterization of the QPC_{6F} devices that we designed (Fig. 1(b)) and we compare the results to our simulations. Figure 5 presents measurements of the conductance G as a function of V_{g1} and V_{g2} . Several labels in the plot illustrate relevant concepts, which were partly discussed before. For the area in this plot with V_{g2} more negative than V_{g1} , we expect some quantum-dot like localization in the middle of the channel and this regime should therefore be avoided in studies of QPC behavior. Further, the plot illustrates that operation for a particular value of L_{eff} requires co-sweeping of V_{g1} and V_{g2} from a particular point below pinch-off in a straight line to the pivot point. This corresponds to opening the QPC at a fixed ratio for V_{g2}/V_{g1} . The pivot point is the point where the gate voltages do not alter the original electron density of the 2DEG. For this measurement, the gate voltage is $V_{g1} = V_{g2} = 0$ V, but this is different for the case of biased cool downs. We carried out biased cool downs for suppressing noise from charge instabilities in the donor layer.^{15,16} For such experiments, the QPCs were cooled down with a positive voltage on the gates.

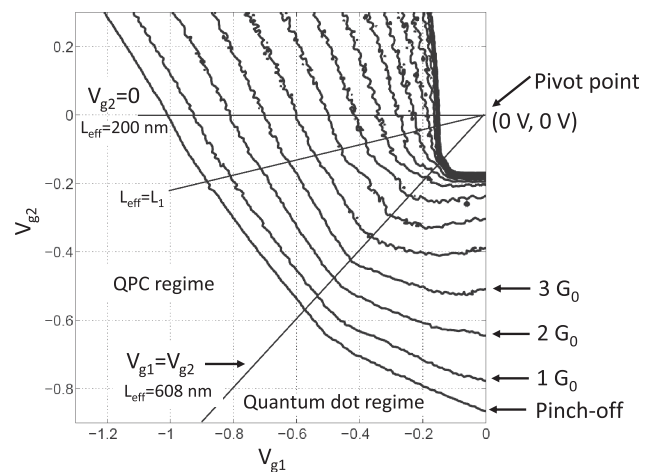


FIG. 5. QPC linear conductance as a function of V_{g1} and V_{g2} for a QPC_{6F} device, presented in the form of iso-conductance lines at integer G_0 levels. The conductance was measured at 4.2 K where the quantized conductance is nearly fully washed out by temperature. The two operational regimes above and below the line $V_{g1} = V_{g2}$ yield QPC and quantum dot behavior, respectively.

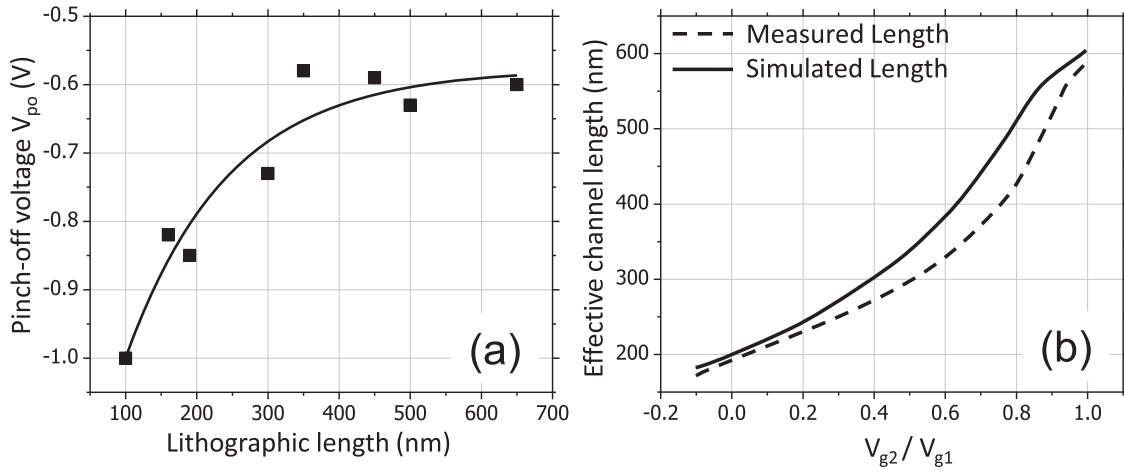


FIG. 6. (a) Experimentally determined relation between the pinch-off gate voltage V_{po} and the lithographic length of QPC_{2F} devices. Points are experimental results. The solid line is a phenomenological expression that was used for parameterizing the relation between V_{po} and the lithographic length. (b) Comparison between measured and simulated values of the effective channel length for a QPC_{6F} device.

We typically used $+0.3$ V and observed indeed better stability with respect to charge noise. The effect of such a cool down can be described as a contribution to the gate voltage of -0.3 V that is frozen into the material.^{15,16} Consequently, co-sweeping of V_{g1} and V_{g2} for maintaining a fixed channel length must now be carried out with respect to the pivot point $V_{g1} = V_{g2} = +0.3$ V instead of $V_{g1} = V_{g2} = 0$ V.

The theory behind the Davies method illustrates why operation at fixed effective length requires a fixed ratio V_{g2}/V_{g1} . All points in the potentials landscapes U for QPC_{2F} devices as in Figs. 3(a) and 3(b) have a height that scales linear with the gate voltage V_g . Thus, when opening the QPC, the full saddle-point potential changes height at a fixed shape. Mimicking this situation with QPC_{6F} devices requires a fixed ratio V_{g2}/V_{g1} , again because V_{g1} and V_{g2} influence U in a linear manner. The plot also illustrates the two special operation lines where the effective length of the channel is unambiguous, and we used these points to better calibrate the relation between V_{g2}/V_{g1} and L_{eff} . The first case is the line at $V_{g2} = 0$, which yields $L_{eff} = 200$ nm, as defined by the central gates alone. The second case is the line $V_{g1} = V_{g2}$. Here, L_{eff} is 608 nm, as defined by the full lithographic length of the 3 gate fingers.

We improved and further checked our calibration of the relation between V_{g2}/V_{g1} and L_{eff} as follows. We used the trend that came out of the simulations (Fig. 4(c)) but pinned the curve at 200 nm for $V_{g2}/V_{g1} = 0$ and at 608 nm for $V_{g2}/V_{g1} = 1$ (black line in Fig. 6(b)). This trace shows good agreement with results from an independent check (dashed line) that used the pinch-off gate voltage V_{po} as an identifier for the effective length. This independent check used data from a set of QPC_{2F} devices for calibrating the relation between L_{litho} and V_{po} (Fig. 6(a)). This shows the trend that shorter QPC_{2F} devices require a more negative gate voltage to reach pinch-off.¹⁷ We related this to the pinch-off values in QPC_{6F} devices. In particular, we analyzed the pinch-off points on the V_{g1} axis, and its dependence on V_{g2}/V_{g1} (see also Fig. 7). The results of using this for assigning a certain L_{eff} to each V_{g2}/V_{g1} is the dashed line in Fig. 6(b) and shows good agreement with the values that were obtained from

simulations. We can thus assign a value to L_{eff} for each V_{g2}/V_{g1} with an absolute error that is at most 50 nm. Notably, the relative error when describing the increase in L_{eff} upon increasing V_{g2}/V_{g1} is much smaller.

The results in Fig. 7 provide an example of linear conductance measurements on a QPC_{6F} device at 80 mK. The traces show clear quantized conductance plateaus for all settings of L_{eff} (Fig. 7(b)). Several of these linear conductance traces also show the 0.7 anomaly (see also Fig. 7(a)), and the strength of its expression shows a modulation as a function of L_{eff} over about 3 periods. This example of control over the 0.7 anomaly illustrates the validity and importance of our type of QPCs in studies of length-dependent transport properties and many-body effects in QPCs. However, a detailed analysis of the observed length dependence goes beyond the scope of the present manuscript. A first detailed study in this direction will be published as Ref. 18.

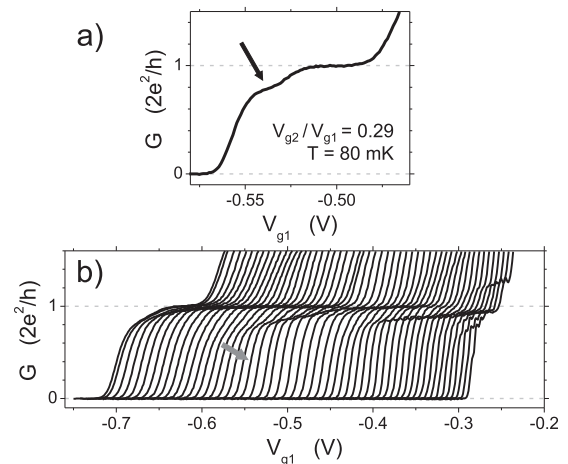


FIG. 7. (a) Linear conductance G as a function of V_{g1} for a QPC_{6F} device with fixed ratio $V_{g2}/V_{g1} = 0.29$, measured at 80 mK. The black arrow points to the 0.7 anomaly in the trace. (b) Linear conductance G measured with the same device and conditions as (a), but now with traces for fixed ratios $V_{g2}/V_{g1} = -0.05$ to $V_{g2}/V_{g1} = 1$ (left to right, traces not offset). This corresponds to increasing the effective channel length L_{eff} from 186 nm to 608 nm. The gray arrow points to the position of the trace that is shown in (a).

VI. CONCLUSIONS

We have developed and characterized length-tunable QPCs that are based on a symmetric split-gate geometry with 6 gate fingers. Gate structures with different shapes and dimensions can be designed depending upon the required range for length tuning and for optimizing the tuning curve. For our purpose (QPCs with an effective channel length between about 200 nm and 600 nm, and 350 nm channel width), we found that simple rectangular gate fingers are an attractive choice. Our simulations and experimental results are in close agreement. We were able to tune the effective length by about a factor 3, from 200 nm to 608 nm. QPCs are the simplest devices that show clear signatures of many-body physics, as, for example, the 0.7 anomaly and the zero-bias anomaly (ZBA).¹⁹ Our length-tunable QPCs provide an interesting platform for systematically investigating these many-body effects. In particular, these QPCs provide a method for studying the influence of the QPC geometry without suffering from device-to-device fluctuations that hamper such studies in conventional QPCs with 2 gate fingers. Studies in this direction are presented in Ref. 18.

ACKNOWLEDGMENTS

We thank Y. Meir for discussions, B. H. J. Wolfs for technical assistance, and the German programs DFG-SPP 1285, Research school Ruhr-Universität Bochum and BMBF QuaHL-Rep 01BQ1035 for financial support. M.J.I. acknowledges a scholarship from the Higher Education Commission of Pakistan.

- ¹B. J. van Wees, H. van Houten, C. W. J. Beenakker, J. G. Williamson, L. P. Kouwenhoven, D. van der Marel, and C. T. Foxon, *Phys. Rev. Lett.* **60**, 848 (1988).
- ²D. A. Wharam, T. J. Thornton, R. Newbury, M. Pepper, H. Ahmed, J. E. F. Frost, D. G. Hasko, D. C. Peacock, D. A. Ritchie, and G. A. C. Jones, *J. Phys. C* **21**, L209 (1988).
- ³K. J. Thomas, J. T. Nicholls, M. Y. Simmons, M. Pepper, D. R. Mace, and D. A. Ritchie, *Phys. Rev. Lett.* **77**, 135 (1996).
- ⁴A. P. Micolich, *J. Phys.: Condens. Matter* **23**, 443201 (2011).
- ⁵T. Rejec and Y. Meir, *Nature* **442**, 900 (2006).
- ⁶E. J. Koop, A. I. Lerescu, J. Liu, B. J. van Wees, D. Reuter, A. D. Wieck, and C. H. van der Wal, *J. Supercond. Novel Magn.* **20**, 433 (2007).
- ⁷D. H. Cobden, N. K. Patel, M. Pepper, D. A. Ritchie, J. E. F. Frost, and G. A. C. Jones, *Phys. Rev. B* **44**, 1938 (1991).
- ⁸J. A. Nixon and J. H. Davies, *Phys. Rev. B* **41**, 7929 (1990).
- ⁹J. H. Davies, I. A. Larkin, and E. V. Sukhorukov, *J. Appl. Phys.* **77**, 4504 (1995).
- ¹⁰G. L. Snider, I. H. Tan, and E. L. Hu, *J. Appl. Phys.* **68**, 2849 (1990).
- ¹¹M. Chen, W. Porod, and D. J. Kirkner, *J. Appl. Phys.* **75**, 2545 (1994).
- ¹²S. E. Laux, D. J. Frank, and F. Stern, *Surf. Sci.* **196**, 101 (1988).
- ¹³J. A. Nixon and J. H. Davies, *Phys. Rev. B* **43**, 12638 (1991).
- ¹⁴E. J. Koop, M. J. Iqbal, F. Limbach, M. Boute, B. J. van Wees, D. Reuter, A. D. Wieck, B. J. Kooi, C. H. van der Wal, e-print arXiv:0809.0928.
- ¹⁵M. Pioro-Ladrière, J. H. Davies, A. R. Long, A. S. Sachrajda, L. Gaudreau, P. Zawadzki, J. Lapointe, J. Gupta, Z. Wasilewski, and S. Studenikin, *Phys. Rev. B* **72**, 115331 (2005).
- ¹⁶C. Buizert, F. H. L. Koppens, M. Pioro-Ladrière, H.-P. Tranitz, I. T. Vink, S. Tarucha, W. Wegscheider, and L. M. K. Vandersypen, *Phys. Rev. Lett.* **101**, 226603 (2008).
- ¹⁷H.-M. Lee, K. Muraki, E. Y. Chang, and Y. Hirayama, *J. Appl. Phys.* **100**, 043701 (2006).
- ¹⁸M. J. Iqbal, E. J. Koop, J. B. Dekker, J. P. de Jong, J. H. M. van der Velde, D. Reuter, A. D. Wieck, R. Aguado, Y. Meir, and C. H. van der Wal, (unpublished).
- ¹⁹S. M. Cronenwett, H. J. Lynch, D. Goldhaber-Gordon, L. P. Kouwenhoven, C. M. Marcus, K. Hirose, N. S. Wingreen, and V. Umansky, *Phys. Rev. Lett.* **88**, 226805 (2002).